On Fault-Mode Phenomenon in No-Insulation Superconducting Magnets: A Preventive Approach

Fangliang Dong[1], Dongkeun Park[1,a)], Wooseung Lee[2], Luning Hao[3], Zhen Huang[4], Juan Bascuñán[1], Zhijian Jin[4], and Yukikazu Iwasa[1]

[1]Francis Bitter Magnet Laboratory/Plasma Science and Fusion Center, Massachusetts Institute of Technology, Cambridge, MA 02139, USA.
[2]Gwangju Center, Korea Basic Science Institute, 77 Yongbong-ro, Buk-gu, Gwangju 61186, Korea.
[3]Electrical Engineering Division, Department of Engineering, University of Cambridge, Cambridge, CB3 0FA, U.K.
[4]School of Electronic Information and Electrical Engineering, Shanghai Jiao Tong University, Shanghai 200240, China.
[a)]Corresponding author email: dk_park@mit.edu

Here we present experimental and analytical results of a preventive approach applied to a fault-mode phenomenon caused by electrodes or power-source failure in a no-insulation (NI) high-temperature superconducting REBCO magnet. It is generally agreed that the NI magnets, at least those of laboratory scale, are self-protected from overheating and therefore from quenching, chiefly because of turn-to-turn current bypassing unique to NI. However, these NI magnets do experience unexpected quenches, e.g., when the current through the magnet suddenly drops due to the aforementioned fault-mode phenomenon. Here, we report this phenomenon of a sudden-discharging-triggered quench of an NI REBCO coil, conduction-cooled and operated at 4.2 K. We also present our preventive approach for this phenomenon that relies on an appropriately designed resistor shunted across the coil terminals. With this shunt resistor, a quench was prevented by suppressing the quench initiating turn-to-turn heat and induced overcurrent within the NI winding, and the coil current decayed safely.

Protection is one of the most challenging issues in the operation of the high-temperature superconducting (HTS) magnet due to its slow normal-zone propagation velocity and consequent difficulty in early-stage quench detection. The no-insulation (NI) winding technique using HTS conductors was first introduced by Hahn *et al*[1] and has been demonstrated its self-protecting characteristics against overcurrent and overheating[2-6]. The key idea of the self-protection in the NI technique is to remove turn-to-turn insulation within the HTS winding and to allow, in the case of a hot spot occurs, the current to be bypassed and the energy to be released through the turn-to-turn contact, which can prevent overheating and consequential permanent burn-out on the hot spot[7, 8]. Besides the self-protecting characteristic, removal of the insulation and reduction of the amount of copper matrix by the NI technique also enables highly compact HTS magnets with larger current densities. Thus, the NI technique has been considered a promising and enabling technology for various magnet applications such as electrical devices[9-11], high-speed transportations[12, 13], nuclear magnetic resonances (NMR)[14-16], energy storages[17], magnetic resonance imaging (MRI)[18-20], and fusion reactors[21, 22], etc.

The NI HTS magnets are relatively safe and reliable against local hot spots or small defects in the superconducting conductors, possibly causing burn-out and quench in conventional insulated magnets. However, we have experienced quenches in NI magnets at some point when the supplying current through the magnets suddenly drops in specific operating conditions (i.e., sudden discharging). The quenches in NI magnets reported so far have occurred mostly during the magnet energizing process[23-26], which appeared to be caused by any types of defects, and these energizing quenches may be avoided by some appropriate designs and approaches[27-30], whereas the sudden-discharging quench reported here can occur at any time due to unexpected external faults such as electrode damages or power-supply failures even if the NI magnet itself is well-designed, non-defective, and well-operated. As the compact high-field NI HTS magnets are designed to operate with a high current density at low temperature to maximize their performance and cost effectiveness, the quench energy margin is relatively small and space for cooling may be limited within the magnet structure

that increase the risk of quench by external faults like sudden discharging. Once the quench initiates, very high induced current fluctuations in the entire NI magnet that are magnetically coupled can cause a cascading entire magnet quench and mechanically damage the magnet by unbalanced force and excessive hoop stresses, as also seen in the quench case of our previous three-nested-coil 18.8-Tesla NI HTS magnet [25, 26].

Therefore, we believe that proper protection is necessary for NI HTS magnets against the quench caused by unexpected and sometimes unavoidable external fault modes. Here, we focus on one of the very severe external fault modes - the external power supply failure that suddenly drops the current directly to zero. In this paper, we have first experimentally and analytically demonstrated this quench by the external power shut-down to understand its mechanism. Then, we introduced and validated the proposed approach to prevent this quench by using an external shunt resistor across the magnet terminals. The external shunting can provide an energy-releasing path in addition to the existing turn-to-turn current-bypassing path in the NI windings.

To demonstrate the proposed quench preventative approach, we used an NI HTS coil as shown in Fig. 1, and conducted the following Steps: (1) sudden discharge the coil without a shunt resistor at different initial operating current levels to reproduce the quench; (2) simulate the transient quench dynamics by using finite element method to understand the mechanism; (3) attach selected-value shunt resistors across the current terminals in parallel with the NI coil and sudden discharge the shunted coil as in Step (1); and (4) compare the experimental and simulated results with a shunt resistor to explain the quench prevention mechanism and mechanical improvements.

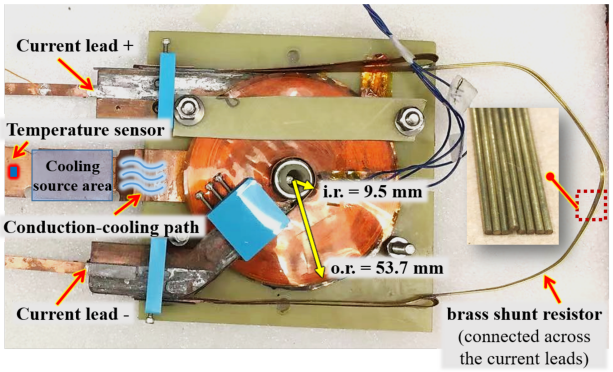

FIG. 1. Photo of the NI HTS coil used for demonstration. This pancake coil has 655 turns wound with 65-μm-thick, 6-mm-wide HTS REBCO (RE: Rare Earth) conductor. All the tests were carried out at an initial temperature of ~4.2 K in the conduction-cooling test rig. The inductance and turn-to-turn contact resistance are 20.9 mH and 4.78 mΩ, respectively. Two brass shunt resistors of ~3.79 mΩ and ~1.92 mΩ were selected to compare their effects during the quench.

For Step (1) without a shunt resistor, we energized the coil to a predetermined initial current I_{ini} and waited for the magnetic field and temperature settlement before cutting off the power supply current by a knife switch. The magnetic field at the coil center, which can represent the NI coil current, was recorded. We repeated tests with increasing I_{ini} from 100 A to 350 A, and the results are shown in Fig. 2. A quench, i.e., a rapid field drop to zero within only ~450 ms, occurred at I_{ini} = 350 A, whereas the fields decayed exponentially with a time constant $\tau \approx 4.37$ s in the cases of I_{ini} = 100-300 A without quenches.

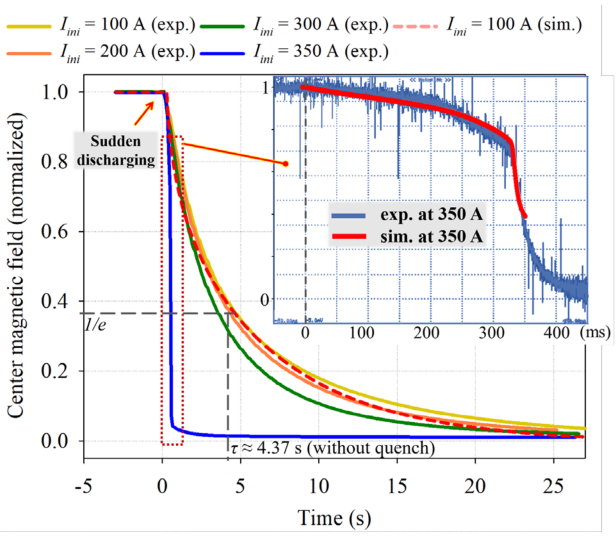

FIG. 2. The recorded coil center fields decay in sudden discharging tests without a shunt resistor. Insert: detailed quench process. Where the simulated result will be described in Step (2).

For Step (2), we established a model fully coupled with electromagnetic, thermal, and mechanical simulations to reveal the quench dynamics in the NI coil. The electromagnetic model is constructed in the frame of *H*-formulation[31], which originally simulates the conventional insulated HTS coils without radial turn-to-turn current flows. For the simulation in this paper, based on rotated anisotropic resistivity[32], we improved the model and enabled it to account for the radial turn-to-turn current flow in an NI coil - it is unachievable by a regular *H*-formulation model. As shown in Fig. 3(a), the 655-turn demonstrative NI coil originally built turn by turn in the model with dense simulation intensity required, is simplified here to six homogenized 2D parts while keeping accurate results by the homogenization method[33]. We have shown the simulated results in Fig. 2 and compared them with the experiments both in the quenched and unquenched cases, confirming the simulation are trustable and in good agreement with the experimental results.

Fig. 3(b) and 3(c), respectively, show the simulated sudden-discharging quench dynamics within each winding part including 1) coil currents in the φ direction (I_{coil}) and the corresponding critical currents (I_C), and 2) the temperatures. After cutting off the power supply circuit at 5 ms, I_{coil} decay in winding part I is observed to be the fastest. This is because the winding part I has the lowest inductance L and the highest turn-to-turn resistance R_C compared to those of the other winding parts, resulting in the fastest exponential decay time constant $\tau = L / R_C$. And because of turn-to-turn joule heat, the temperature rising in the winding part I is also the fastest. However, I_{coil} decay in the winding part I does not mean a quench happens in this time range (t = [5 ms, ~90 ms]). Then, due to thermal diffusion, the winding part II is heated, leading to its I_C degradation faster than its I_{coil} decay. At the moment of $t_1 \approx 90$ ms in Fig. 3(b), we believe the partial quench initiates, as I_C drops lower than I_{coil} in the winding part II, i.e., the I_{coil} and I_C curves have overlapped area colored in orange shadow in the figure. Due to electromagnetic coupling and flux conservation, I_{coil} in parts III-VI rises in a sequence exceeding its corresponding I_C and then quenches just as the overlapped areas with colored shadows indicated in the figure. The quench happens like an avalanche spreading towards the outermost winding part, with increasing overcurrent level and propagation speed. Finally, at $t_4 \approx 345$ ms, all of the shadows are overlapped, indicating the entire coil is quenched.

For a more detailed revelation of the quench propagation, we show the normalized coil current density (J_{coil}) distributions in the winding at typical time points, as the plots shown in Fig. 3(b). We can see that the quenched area (i.e., red area) pushes and squeezes the superconducting area (i.e., yellow and green areas) towards the outermost winding part and finally fills out all of the winding. Also, as the plots shown in Fig. 3(c), the heat moves with the quench propagation and accumulates, forming a hottest spot in the outermost winding part at t = 345 ms.

We calculated the quench in radial propagation is 0.17 m/s, and concluded that the sudden-discharging-triggered quench is initiated by turn-to-turn heat even when $I_{coil} < I_C$, and then the quench is spread out by induced overcurrent. Whereas the currently widely reported energizing quench[23-26] happens when $I_{coil} > I_C$ due to local defects - a totally different mechanism to our reported quench in this paper.

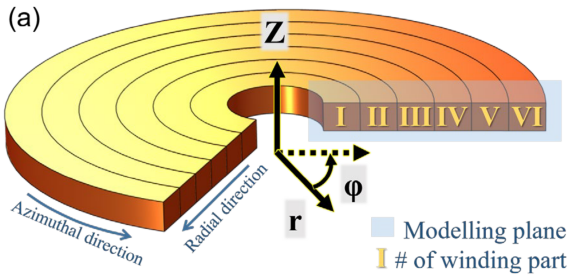

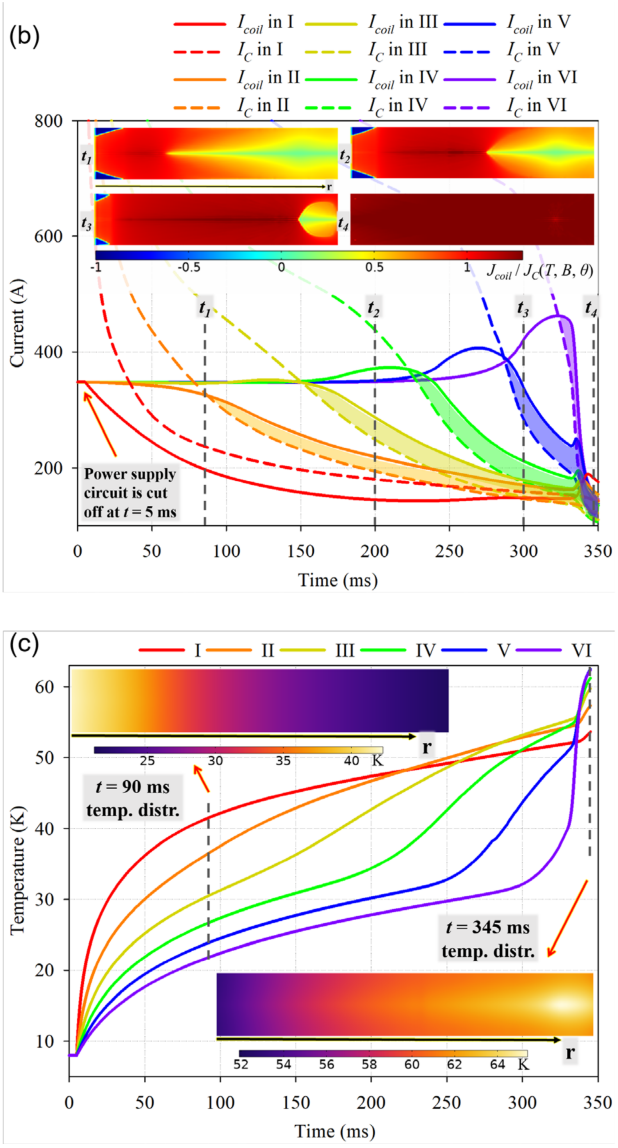

FIG. 3. The simulation for the quench dynamics. (a) The 2D homogenized model. It is divided into 6 winding parts, #I-VI, but all of the physical variables keep continuous between parts. (b) Changes of coil currents (I_{coil}) and corresponding critical currents (I_C) during the quench process. The shadows are the overlaps of I_C and I_{coil} curves, which indicate quenches. The plots in the figure are the winding current density (J_{coil}) distributions (normalized by $J_C(T,B,\theta)$, the local temperature T- and anisotropic θ- field B-dependent critical current density). Quench happens when the legend >1. (c) Changes of temperatures in the quench process. The plots in the figure are temperature distributions.

According to the simulation in Step (2), the key point of this quench prevention is to avoid initial heat generated by the turn-to-turn current - this is also the preferential consideration in the selection of an appropriate shunt resistor. That is, the portion of the in-winding current diverted by the external bypassing must be significant enough in order to suppress the turn-to-turn joule heat to be always lower than the cooling capacity during the sudden discharging. The macroscopic electrical behaviors of the shunted NI coil including the amount of diverted current are governed by a circuit model, which consists of a shunt resistor and lumped equivalent circuits of each NI winding part, as shown in Fig. 4(a). The effect of shunting mainly relates to cooling condition, turn-turn heating, and magnetic coupling in NI winding.

For Step (3), considering the rated cooling capacity of the cryocooler we used (Sumitomo RDK-408D2: 1 W at 4.2 K and 50 W at 43 K) and turn-to-turn contact resistance $R_C \approx 4.78$ mΩ, we first estimated the initial maximum turn-to-turn current in the winding has to be lower than 102 A base on the joule heat equation (i.e., 102 A×102 A×4.78 mΩ < 50 W) - this indicates the external shunting needs to divert at least 248 A (i.e., 350-102=248 A). Therefore, the corresponding shunt resistance is calculated to be 1.97 mΩ (i.e., 248 A/102 A ≈ R_C/1.97 mΩ). To fast while safely release the energy by the shunt, inductive magnet terminal voltage also needs to be considered. With this shunting, ~0.5 V is calculated - this is acceptable for the demonstrative coil because the inductance is not very large. In the test, we used two external shunt resistors measured R_{sh1} = 3.79 mΩ and R_{sh2} = 1.92 mΩ, the latter is set as close as the calculated value, and the former is set about twice larger for effect comparison.

The sudden discharging tests on the shunted coil with I_{ini} = 350 A are shown in Fig. 4(b). With R_{sh1}, the quench still occurs but is delayed to ~2 s, more than 4 times longer compared to that of the unshunted case. The longer the quench is delayed, the less the initial quench energy remains, and thus the lower the damage risk would be. While with R_{sh2}, the quench is completely eliminated, and the coil center field decays exponentially with an average $\tau \approx 15.28$ s. Fig. 4(b) also shows the simulated diverted current in R_{sh2}, it is ~260 A at the beginning, meeting the required >248 A estimated above, and suppressing the initial turn-to-turn heat.

Under the given resistance of 1.92 mΩ, we adopt 8 round brass rods connected in parallel as the shunt resistor. Each rod has 1-mm diameter and 23-cm length.

Compared to copper and stainless steel, brass has better thermal and electrical stability while transporting the diverted current under adiabatic heating condition. After the test, the final temperature on the brass shunt is estimated to be <240 K[34].

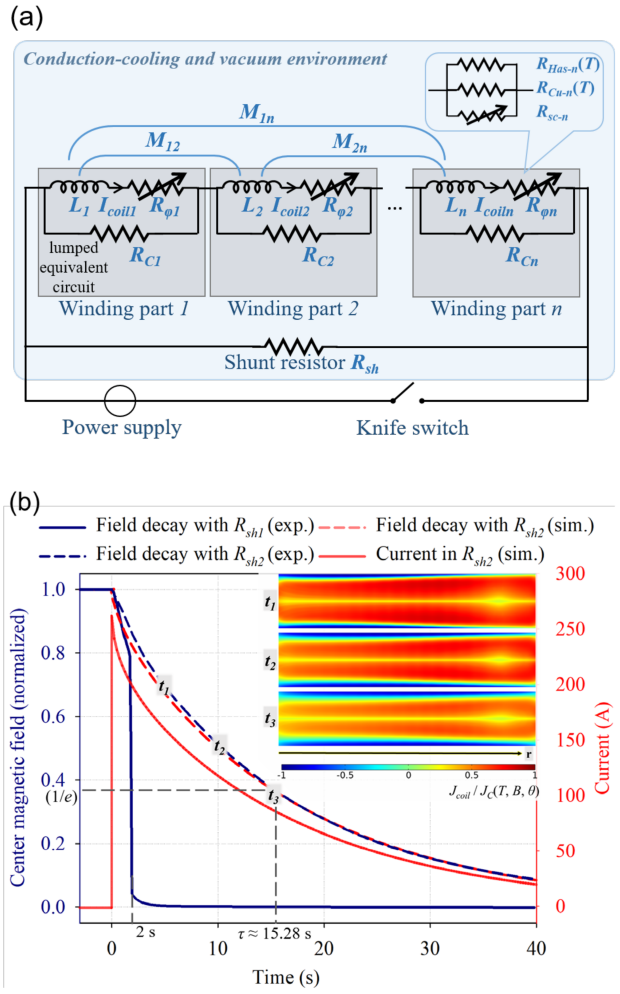

FIG. 4. For the shunted coil, (a) its governing circuit model has inductors including both self- and mutual-inductances (L and M), with azimuthal REBCO conductor resistors (R_φ) connecting in series and turn-to-turn contact resistors (R_C) connecting in parallel. Where R_φ mainly has three components: R_{has} from the Hastelloy layer, R_{cu} from the copper stabilizer, and R_{sc} from the superconductor. (b) The sudden discharging results with 350 A initial current. With the 1.92 mΩ shunting (R_{sh2}), the quench is completely eliminated. Plots: the normalized winding current density distributions at typical time points show no quenches during the entire discharging.

In Step (4), with the shunt resistor R_{sh2} in place, we again simulated the normalized current density distributions and the temperature changes within the winding (Fig. 4(b) the inserted plots and Fig. 5, respectively). From the results, the normalized current density distributions at typical time points 5 s (t_1), 10 s (t_2), and 15.28 s (t_3, i.e., τ) indicate the coil has no induced overcurrent exceeding the critical current, and consequentially, no quench during the entire sudden-discharging process. The maximum temperature reached is ~39 K, which is much lower than that of the unshunted case in Fig. 3(c). Through Steps (3) and (4), we proved that the proposed external shunt resistor suppresses the turn-to-turn heat and the induced overcurrent during the sudden discharging, maintaining the superconducting region in the winding without quench. Moreover, we compared the winding stress induced by electromagnetic forces (e.g., the radial stress in Fig. 6). Simulation results show the maximum stress reduces from 428 MPa during quench down to 115 MPa without quench, which proves that the proposed external shunting can mechanically protect the coil as well. This mitigation of force fluctuation is essential to operation safety, especially for large-scale magnets.

Note that this shunting concept intrinsically results in a longer time constant, here, 15.28 s (shunted) and 4.37 s (unshunted), and thus longer time to energize the magnet.

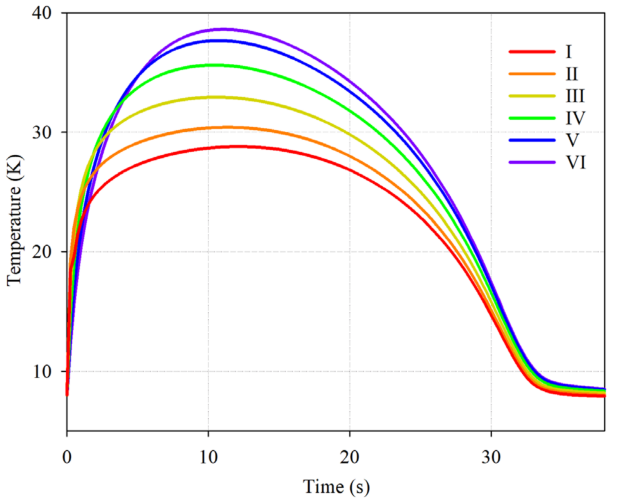

FIG. 5. Winding temperature changes when applied with a shunt resistor R_{sh2}.

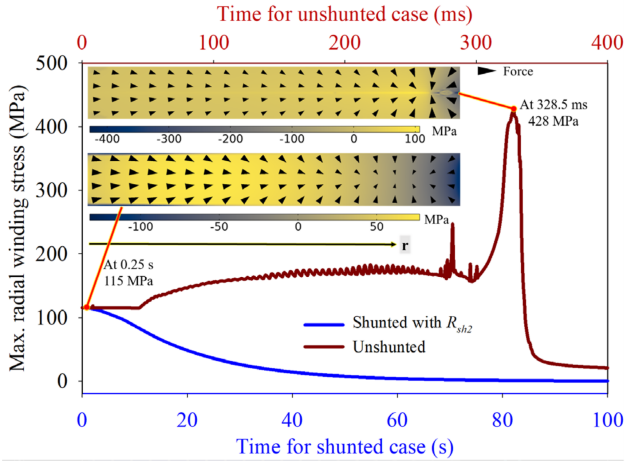

FIG. 6. The maximum radial winding stress simulated in the cases of shunted and unshunted. The stress during quench (i.e., the brown line) has a high peak at 328.5 ms due to rapid electromagnetic fluctuations in the winding without shunting. Plots: forces and stress distributions at the maximum values, for the shunted case, at 0.25 s (the lower plot), and for the unshunted case, at 328.5 ms (the upper plot).

In conclusion, a preventive approach against sudden-current-discharging quench, a fault-mode phenomenon in NI HTS magnets, is proposed and demonstrated both experimentally and analytically. Based on the validated simulation model, the turn-to-turn joule heat in the inner winding parts initiates a partial quench, and then the induced overcurrent fast spreads out the partial quench towards the outer winding parts, resulting in an entire quench within the NI coil. The external shunt resistor, as the key idea in this proposed preventive approach, is made of thin brass rods for thermally and electrically stable operation during the quench. This external shunt resistor can effectively reduce the joule heat (i.e., the quench initiator) by bypassing the winding current, and then suppresses the induced current (i.e., the quench spreader) not to exceed the critical current, remaining sufficient superconducting areas within the winding for a safe coil discharging without a quench. Meanwhile, the risk of mechanical damage in the quench is also significantly reduced. To extrapolate this shunt resistor to a more general magnet, first, estimate the needed diverted current based on the specific cooling condition, then determine the shunt resistance based on the diverted current and the turn-to-turn contact resistance, at last, if the discharging voltage of the magnet is still too high, then further reduce the shunt resistance. In practical applications, this fault-mode phenomenon preventive approach has the advantage of being able to add, adjust, or replace the shunt resistor even after completing and pre-testing the main magnet, this is impossible with a conventional NI HTS magnet. It is also very convenient just by adding this shunt resistor across the two electrodes (i.e., the current leads) can have the magnet protected. We believe the above merits enable the proposed preventative approach highly compatible and practically applicable for quench prevention in most NI HTS magnets.

This work was supported by the National Institute of General Medical Sciences of the National Institutes of Health under Award R01GM137138. The authors thank Pu Duan and Jingdong Li, from the School of Electrical and Electronic Engineering, Huazhong University of Science and Technology, Wuhan, China, for important suggestions on modeling. The authors also thank the support from SJTU Scholarship.

DATA AVAILABILITY

The data that support the findings of this study are available from the corresponding author upon reasonable request.

REFERENCES

1. S. Hahn, D. K. Park, J. Bascunan and Y. Iwasa, IEEE T Appl Supercon **21** (3), 1592-1595 (2011).
2. Y. Suetomi, T. Yoshida, S. Takahashi, T. Takao, G. Nishijima, H. Kitaguchi, Y. Miyoshi, M. Hamada, K. Saito, R. Piao, Y. Takeda, H. Maeda and Y. Yanagisawa, Supercond Sci Tech **34** (6) (2021).
3. F. L. Dong, Z. Huang, X. F. Li, L. N. Hao, L. P. Yao, W. Wu and Z. J. Jin, IEEE T Appl Supercon **29** (5) (2019).
4. D. H. Liu, W. W. Zhang, H. D. Yong and Y. H. Zhou, Supercond Sci Tech **31** (8) (2018).
5. J. B. Song, S. Hahn, T. Lecrevisse, J. Voccio, J. Bascunan and Y. Iwasa, Supercond Sci Tech **28** (11) (2015).
6. S. Hahn, Y. Kim, D. K. Park, K. Kim, J. P. Voccio, J. Bascunan and Y. Iwasa, Appl Phys Lett **103** (17) (2013).
7. W. K. Chan and J. Schwartz, Supercond Sci Tech **30** (7) (2017).
8. Y. Wang, W. K. Chan and J. Schwartz, Supercond Sci Tech **29** (4) (2016).
9. U. Bong, C. Im, J. Yoon, S. An, S. W. Jung, K. J. Han and S. Hahn, IEEE T Appl Supercon **31** (5) (2021).
10. F. Schreiner, Y. Z. Liu, Y. Z. Zhang, R. Gyuraki, M. Noe and M. Doppelbauer, IEEE T Appl Supercon **30** (4) (2020).
11. D. Qiu, Z. Y. Li, F. Gu, Z. Huang, A. Zhao, D. Hu, B. G. Wei, H. Huang, Z. Hong, K. Ryu and Z. Jin, Physica C **546**, 1-5 (2018).
12. X. Y. Teng, Z. Huang, F. L. Dong, X. Y. Xu, Z. J. Jin, Y. Shi, A. F. Zhao, X. Z. Yuan and Y. X. Feng, IEEE T Appl Supercon **31** (5) (2021).

13. F. L. Dong, Z. Huang, L. N. Hao, X. Y. Xu, Z. J. Jin and N. Shao, Sci Rep-Uk **9** (2019).
14. D. Park, Y. H. Choi and Y. Iwasa, IEEE T Appl Supercon **29** (5) (2019).
15. Y. Iwasa, J. Bascunan, S. Hahn, J. Voccio, Y. Kim, T. Lecrevisse, J. Song and K. Kajikawa, IEEE T Appl Supercon **25** (3) (2015).
16. T. M. Qu, P. C. Michael, J. Voccio, J. Bascunan, S. Hahn and Y. Iwasa, Appl Phys Lett **109** (8) (2016).
17. Y. Miyamoto, A. Ishiyama, W. Tomonori and N. Shigeo, IEEE T Appl Supercon **32** (6) (2022).
18. T. Wang, H. Quan, L. Chen, K. Z. Ding, S. S. Du and C. L. Zou, IEEE T Appl Supercon **31** (8) (2021).
19. Y. Li and S. Roe, Supercond Sci Tech **34** (12) (2021).
20. K. L. Kim, J. B. Song, Y. H. Choi, D. G. Yang and H. Lee, IEEE T Appl Supercon **27** (4) (2017).
21. Y. H. Zhai, B. Berlinger, C. Barth and C. Senatore, Supercond Sci Tech **34** (10) (2021).
22. N. Mitchell, J. X. Zheng, C. Vorpahl, V. Corato, C. Sanabria, M. Segal, B. Sorbom, R. Slade, G. Brittles, R. Bateman, Y. Miyoshi, N. Banno, K. Saito, A. Kario, H. Ten Kate, P. Bruzzone, R. Wesche, T. Schild, N. Bykovskiy, A. Dudarev, M. Mentink, F. J. Mangiarotti, K. Sedlak, D. Evans, D. C. Van Der Laan, J. D. Weiss, M. Liao and G. Liu, Supercond Sci Tech **34** (10) (2021).
23. K. R. Bhattarai, K. Kim, K. Kim, K. Radcliff, X. B. Hu, C. Im, T. Painter, I. Dixon, D. Larbalestier, S. Lee and S. Hahn, Supercond Sci Tech **33** (3) (2020).
24. Y. Li, D. Park, Y. F. Yan, Y. Choi, J. Lee, P. C. Michael, S. W. Chen, T. M. Qu, J. Bascunan and Y. Iwasa, Supercond Sci Tech **32** (10) (2019).
25. D. Park, J. Bascunan, P. C. Michael, J. Lee, Y. H. Choi, Y. Li, S. Hahn and Y. Iwasa, IEEE T Appl Supercon **29** (5) (2019).
26. P. C. Michael, D. Park, Y. H. Choi, J. Lee, Y. Li, J. Bascunan, S. Noguchi, S. Hahn and Y. Iwasa, IEEE T Appl Supercon **29** (5) (2019).
27. G. T. Ma, T. Y. Gong, R. C. Wang, S. L. Li, X. C. Nie, P. B. Zhou, J. Li, C. Li, Z. F. Ge and H. B. Cui, Supercond Sci Tech **35** (2) (2022).
28. D. Park, J. Bascunan, Y. Li, W. Lee, Y. Choi and Y. Iwasa, IEEE T Appl Supercon **31** (5) (2021).
29. Y. H. Wang, Q. L. Wang, J. H. Liu, J. S. Cheng and F. Liu, Supercond Sci Tech **33** (6) (2020).
30. S. Noguchi, IEEE T Appl Supercon **29** (5) (2019).
31. B. Y. Shen, F. Grilli and T. Coombs, IEEE Access **8**, 100403-100414 (2020).
32. R. C. Mataira, M. D. Ainslie, R. A. Badcock and C. W. Bumby, Supercond Sci Tech **33** (8) (2020).
33. V. M. R. Zermeno, A. B. Abrahamsen, N. Mijatovic, B. B. Jensen and M. P. Sorensen, J Appl Phys **114** (17) (2013).
34. Y. Iwasa, *Case Studies in Superconducting Magnets: Design and Operational Issues*, 2nd ed. (Springer, 2009).